High spin behavior of ^{153}Eu

Somapriya Basu, S. Chattopadhyay, and J. M. Chatterjee
Saha Institute of Nuclear Physics, 1/AF Bidhannagar, Calcutta 700 064, India

R. K. Chattopadhyay
Physics Department, A. M. College, 102/1 Amherst Street, Calcutta 700 009, India

S. S. Ghugre
Physics Department, Bombay University, Vidyanagari, Bombay 400 089, India

G. Rodrigues, R. P. Singh, S. Murulithar, and R. K. Bhowmik
Nuclear Science Center, Aruna Asaf Ali Marg, New Delhi 110 067, India
(Received 6 May 1996)

The high-spin behavior of ^{153}Eu nucleus has been investigated via the ^{150}Nd(^{7}Li,$4n\gamma$) reaction. The level structures of the nucleus built on the $5/2^+$ ground state and the $5/2^-$ excited state have been established up to spins $39/2^+$ and $43/2^-$, respectively, and are observed to be interleaved through strong $E1$ transitions. From the $B(E1)/B(E2)$ ratios of the high-spin region the intrinsic electric-dipole moment is deduced and is found to be 0.181 ± 0.007 e fm and β_3 thus obtained is ~ 0.03. The rotational features and magnetic moments indicate that an octupole correlated deformation has developed with the increasing spin. A theoretical study of the correlation between the β_3 and the band crossing frequency supports the conjecture of octupole deformation at high spin. [S0556-2813(97)00910-2]

PACS number(s): 21.10.Re, 21.60.Cs, 23.20.−g, 27.70.+q

I. INTRODUCTION

The ^{153}Eu ($Z=63$, $N=90$) nucleus lies in the transitional rare-earth region where nuclei are neither spherical nor well deformed. The nuclei of this region exhibit a strong interplay between single-particle and collective excitations. This manifests itself in various interesting phenomena, e.g., backbending or upbending, band crossing, and the enhancement or reduction of single-particle alignment. In ^{153}Eu, [$\pi d_{5/2}$; $\pi h_{11/2}$] and [$\nu f_{7/2}$; $\nu i_{13/2}$] orbitals are very close to the proton and neutron Fermi levels, respectively. With increasing deformation the odd proton occupies the high-j $h_{11/2}$ orbital, giving rise to the low-lying negative-parity deformed states. Although a previous study reports that at low excitation, there is a very small interaction between the particles through the Y_{30} term of the Hamiltonian [1], experimental results show that the opposite-parity levels are interconnected through strong $E1$ transitions until $J^\pi=35/2^\pm$ spin states [2]. In Ref. [2] the reported positive-parity ground-state band, the negative-parity band built on $5/2^-$, and the sideband built on $3/2^+$ were extended to the 3270.3 keV ($J^\pi=35/2^+$), 3103.0 keV ($J^\pi=35/2^-$), and 2082.8 keV ($J^\pi=25/2^+$) states, respectively. Here we shall present the results of the investigation of the characteristics of the high spin states in the higher excited region of ^{153}Eu.

II. EXPERIMENT

The nucleus ^{153}Eu was produced by bombarding a 4 mg/cm^2 thick ^{150}Nd target (96.6%) with a ^{7}Li beam at $E_{\rm proj}\sim 36$ MeV provided by the 15UD pelletron accelerator of the Nuclear Science Center, New Delhi. The preparation of the target is described in Ref. [3]. The target was then pasted on a 4 mg/cm^2 thick mica sheet to protect it from any possible damage due to heat.

The γ rays were detected in the gamma-detector array (GDA). This array consisted of six Compton suppressed hyperpure germanium (HPGe) detectors and a 14-element bismuth germanate multiplicity filter at the time of this experiment. Three of the HPGe detectors were positioned at 99° and the remaining three at 153° with respect to the beam axis. The details of the GDA setup with the associated electronics has already been reported [4]. Altogether 3×10^7 events have been collected and sorted off-line to form two two-dimensional 4096×4096 E_γ-E_γ matrices. One of the matrices was for γ-γ coincidences and the other for ratios of the directional correlations of the oriented nuclear states (DCO). The competing channels of the ^{150}Nd(^{7}Li,xn) reactions computed with the CASCADE code at 36 MeV are ^{150}Nd(^{7}Li,$4n$)^{153}Eu and ^{150}Nd(^{7}Li,$5n$)^{152}Eu. The production of the ^{153}Eu nucleus is 73% of the total reaction cross section.

The DCO ratios were calculated according to the relation

$$R_{\rm DCO}=\frac{I_\gamma(\text{at } 99^\circ \text{ gated by } \gamma \text{ ray at } 153^\circ)}{I_\gamma(\text{at } 153^\circ \text{ gated by } \gamma \text{ ray at } 99^\circ)}. \qquad (1)$$

Transitions having DCO ratios in the range 0.9–1.1 with a mean value 0.98, when gated with a stretched $E2$ transition, are assigned multipolarity 2. The DCO ratios of dipole transitions lie in the range 1.6–2.2. Their mean value is found to be 1.80. The energies and DCO ratios obtained for the γ transitions in the present work agree quite well with the result reported by Pearson *et al.* [2]. The intensities of the transitions are in reasonable agreement with those of Ref. [2], especially in the low-spin region. For the high-spin levels

TABLE I. Energy and intensity of γ rays and DCO ratios observed.

E_γ (keV)	Rel. I_γ	DCO	E_γ (keV)	Rel. I_γ	DCO	E_γ (keV)	Rel. I_γ	DCO
53.6±0.8	139.5±6.9	1.27(7)	178.2±0.6	15.4±1.5		393.3±0.7	3.6±0.1	2.1(7)
83.1±0.7	130.9±3.8[a]		193.7±0.6	81.1±2.0	0.96(3)	397.5±0.7	7.4±0.4	
83.3±0.7	21.1±4.2[a]		196.4±0.6	8.8±0.8		406.4±0.7	47.9±2.9	0.99(6)
86.0±0.7	113.1±2.9		200.0±0.6	22.3±3.8[a]	1.80(9)	412.3±0.7	29.9±9.0	0.77(8)
89.6±0.7	9.2±0.3[a]	1.30(7)	200.9±0.6	2.3±0.4[a]		413.1±0.7	11.5±3.4	
96.6±0.7	20.2±1.0[a]		209.6±0.7	6.0±1.1	1.17(7)	423.7±0.7	18.0±2.8	
97.1±0.7	145.0±2.6		222.3+222.4 +222.5	11.3±3.5[a,b]		429.3±0.7	4.9±0.2[a]	1.82(2)
102.6±0.7	1.6±0.2[a]		223.2±0.6	12.9±3.7		436.8±0.7	61.0±1.2	1.02(10)
103.2±0.7	23.1±1.8[a]		232.3±0.6	3.5±1.8	0.71(5)	442.1±0.7	40.2±0.8	1.01(8)
108.3±0.7	4.4±0.8[a]		235.8±0.6	77.0±2.3	1.25(5)	450.2±0.7	74.5±1.1	1.0(7)
109.3±0.7	28.3±5.7[a]		236.8±0.6	8.9±0.3		456.9±0.7	0.9±0.1[a]	1.80(4)
111.3±0.7	28.1±0.6	1.04(9)	241.4±0.6	176.9±5.3[a]	0.90(3)	460.4±0.7	13.6±1.6	
126.4±0.7	5.2±0.8[a]		242.3±0.6	101.4±3.6	0.94(7)	473.2±0.7	43.3±2.6	1.03(9)
126.5±0.7	12.0±0.7[a]		244.5±0.6	5.8±0.3[a]		476.0±0.7	2.8±0.3[a]	
128.5±0.7	39.8±1.6		261.6±0.7	7.4±1.3		481.9±0.8	11.8±1.4[a]	
129.5±0.7	20.8±0.8		263.2±0.7	1.0±0.1		489.7±0.7	10.4±1.3	
131.6±0.7	>8.3		267.5±0.7	84.1±1.7	0.90(8)	504.1±0.8	21.7±2.6	0.96(8)
132.0±0.7	<5.4		267.7±0.7	14.8±0.7		507.2±0.8	1.4±0.1	
137.5±0.7	5.4±2.0		271.7±0.7	9.5±1.6[a]		509.6±0.8	53.5±5.4[a]	1.07(10)
141.5±0.7	12.4±0.8[a]		271.9±0.7	2.2±0.4[a]	2.08(12)	520.8±0.8	62.7±2.5	1.01(8)
142.0±0.7	30.8±5.2[a]	1.64(12)	287.6±0.7	100	1.02(3)	530.9±0.8	23.3±2.1	0.98(8)
146.5±0.7	0.6±0.1		290.8±0.7	1.3±0.6		534.8±0.9	9.5±1.4[a]	
151.4+151.6	178.9±2.7[b]		293.2±0.7	9.6±2.6		556.9±0.8	10.5±0.4	1.08(12)
154.1±0.7	12.4±1.5		302.3±0.7	11.6±1.2		565.6±0.8	38.9±8.6	
155.7±0.6	101.7±2.5		307.2±0.7	37.8±2.7	1.39(11)	574.9±0.8	23.0±2.4[a]	0.96(6)
156.8±0.6	17.5±0.4	0.7(1)	309.6±0.7	0.4±0.1		580.2±0.8	9.5±1.0[a]	0.99(9)
159.6±0.6	13.6±3.4	1.7	310.8±0.7	0.4±0.2		592.1±0.9	11.3±3.4	
162.9±0.6	1.2±0.1[a]		319.9±0.7	11.3±3.1		600.1±0.9	10.9±2.7	1.02(11)
166.3±0.6	65.9±1.7		329.5±0.7	96.1±2.8	0.98(4)	601.2±0.9	5.9±1.8	0.91(9)
170.0±0.6	218.8±3.3[a]	0.93(9)	339.0±0.7	17.5±3.0	1.8(5)	619.8±0.9	6.7±1.7	
170.2±0.6	5.4±0.3[a]	1.5(4)	347.4±0.7	90.1±1.8	0.92(10)	621.6±0.9	3.4±0.5	0.95(2)
174.7±0.6	40.8±3.7[a]		353.2±0.7	11.7±0.3		635.0±0.9	3.3±0.4	0.99(12)
175.6±0.6	5.4±0.3[a]		364.9±0.7	151.4±3.1	1.0(4)	641.3±0.9	1.1±0.1	
176.7±0.6	33.2±4.0[a]	1.5(4)	367.2±0.7	7.0±0.4	1.54(12)	650.9±0.9	0.9±0.1	
177.7±0.6	9.3±0.5[a]		370.3±0.7	83.4±5.8	0.99(5)	690.3±1.0	1.4±0.2	

[a]Intensities tabulated from coincidence spectra.

[b]Combined intensities of the unresolved γ rays.

above $25/2^+$ and $21/2^-$ of the $5/2^\pm$ bands the intensities have not been previously reported. The energies, intensities, and DCO ratios obtained in the present work are given in Table I.

In Fig. 1 the partial level scheme constructed from the γ-γ coincidence relationships and DCO ratios is displayed. The three bands reported previously have been extended to spins $J^\pi = 39/2^+$, $43/2^-$, and $29/2^+$, respectively. The cross transitions connecting opposite-parity energy levels built on $5/2^+$ and $5/2^-$ states persist until the $33/2^+$ spin.

The nonyrast sideband (band 3) built on the $3/2^+$, 103 keV state, extended further to the $29/2^+$ spin, shows a very good rotational character. Unlike the sidebands in other nuclei in this region, this band does not decay to the $5/2^+$ ground-state band through fast $M1$ and/or $E2$ transitions. It is rather interesting to note that besides its intraband transitions, the excited levels of this band decay to the negative parity band via $E1$ transitions.

III. RESULTS

A. Rotational features

The rotational parameters of the $5/2^+$ ground-state positive-parity band and the $5/2^-$ negative-parity band have been calculated using the Harris formulas [5]. The dynamical moment of inertia $\mathcal{J}^{(2)}$ and the aligned angular momentum $i_{\text{s.p.}}$ have been extracted from the observed energies of the excited states of same parity π and signature quantum number α for $5/2^\pm$ bands. The reference angular momentum has been estimated from the inertial parameters $\mathcal{J}_0$ and $\mathcal{J}_1$ calculated from the average value of two neighboring even-even nuclei ^{152}Sm and ^{154}Gd. The values as calculated for these two nuclei are $\mathcal{J}_0 = 23.3\hbar^2/(\text{MeV})$, $\mathcal{J}_1 = 352.7\hbar^4/(\text{MeV}^3)$ and $\mathcal{J}_0 = 23.1\hbar^2/(\text{MeV})$, $\mathcal{J}_1 = 332.9\hbar^4/(\text{MeV}^3)$, respectively.

The plots of $\mathcal{J}^{(2)}$ and $i_{\text{s.p.}}$ with rotational frequency $\hbar\omega$ are shown in Figs. 2(a) and 2(b), respectively. These figures

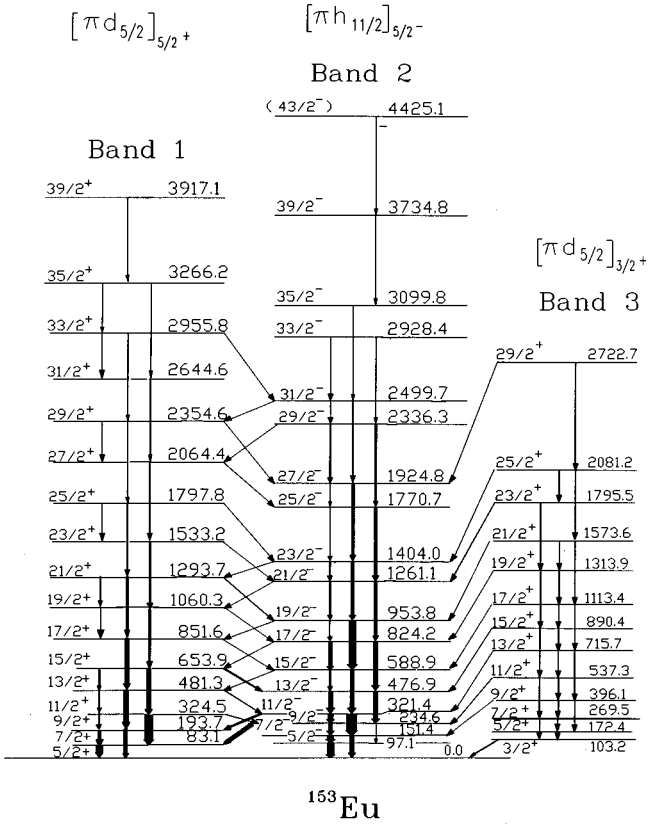

FIG. 1. Partial level scheme of ^{153}Eu showing positive-parity and negative-parity bands; $M1$, $E1$, and $E2$ transitions, connection with an extended sideband built on the $3/2^+$ state.

indicate that there is a large signature splitting and signature dependence of single-particle alignment for band 2, while band 1 shows a rather weak signature splitting and perhaps a signature dependence on the alignment. However, if the $5/2^+$ band (band 1) originates purely from the $d_{5/2}$ orbital, it is not expected to undergo a signature splitting at these rotational frequencies. This weak signature splitting is possible if there is a mixing of high-j orbitals. The calculation of the single-particle energies in a deformed Woods-Saxon potential indicates that the $5/2^+$ orbital of $g_{7/2}$ lies 1.3 MeV higher than the $5/2^+$ orbital of $d_{5/2}$ for $\beta_2=0.2$ and thus mixing through the Y_{20} term is negligible, while the $5/2^-$ orbital of $h_{11/2}$ is almost degenerate (148 keV apart). Thus a small Y_{30} term can lead to a mixing of $5/2^+$ and $5/2^-$ orbitals of $d_{5/2}$ and $h_{11/2}$, respectively.

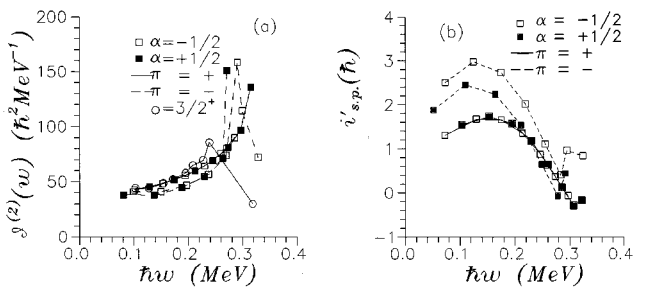

FIG. 2. (a) Dynamical moment of inertia $\mathcal{J}^{(2)}$ for both positive- and negative-parity bands; (b) single-particle angular momentum alignment $i_{\text{s.p.}}(\omega)$ calculated for four bands against rotational energy.

TABLE II. $B(E1)/B(E2)$ ratios for positive bands, negative bands, and sideband.

$E_{\gamma 1}$ (keV)	$E_{\gamma 2}$ (keV)	I_i	$I_f(E1)$	$I_f(E2)$	$B(E1)/B(E2)$ (10^{-6} fm^{-2})
89.6	241.4	$11/2^+$	$9/2^-$	$7/2^+$	0.05 ±0.02
159.6	287.6	$13/2^+$	$11/2^-$	$9/2^+$	0.05 ±0.01
176.7	329.5	$15/2^+$	$13/2^-$	$11/2^+$	0.19 ±0.02
261.6	370.3	$17/2^+$	$15/2^-$	$13/2^+$	0.03 ±0.01
236.8	406.4	$19/2^+$	$17/2^-$	$15/2^+$	0.12 ±0.02
339.0	442.1	$21/2^+$	$19/2^-$	$17/2^+$	0.15 ±0.01
271.7	473.2	$23/2^+$	$21/2^-$	$19/2^+$	0.20 ±0.04
393.3	504.1	$25/2^+$	$23/2^-$	$21/2^+$	0.07 ±0.01
293.2	530.9	$27/2^+$	$25/2^-$	$23/2^+$	0.49 ±0.14
429.3	556.9	$29/2^+$	$27/2^-$	$25/2^+$	0.22 ±0.01
456.9	601.2	$33/2^+$	$31/2^-$	$29/2^+$	0.09 ±0.03
170.2	347.4	$17/2^-$	$15/2^+$	$13/2^-$	0.05 ±0.01
102.6	364.9	$19/2^-$	$17/2^+$	$15/2^-$	0.05 ±0.01
200.9	436.8	$21/2^-$	$19/2^+$	$17/2^-$	0.06 ±0.01
271.9	565.6	$29/2^-$	$27/2^+$	$25/2^-$	0.12 ±0.03
244.5[a]	223.2	$9/2^+$	$7/2^-$	$5/2^+$	0.012±0.004
302.3[a]	267.7	$11/2^+$	$9/2^-$	$7/2^+$	0.03 ±0.01
394.0[a]	319.9	$13/2^+$	$11/2^-$	$9/2^+$	0.03 ±0.01
413.1[a]	353.1	$15/2^+$	$13/2^-$	$1/2^+$	0.06 ±0.02
524.5[a]	397.5	$17/2^+$	$15/2^-$	$13/2^+$	0.05 ±0.01
489.7[a]	423.8	$19/2^+$	$17/2^-$	$15/2^+$	0.05 ±0.01
619.8[a]	460.4	$21/2^+$	$19/2^-$	$17/2^+$	0.03 ±0.01
534.4[a]	481.9	$23/2^+$	$21/2^-$	$19/2^+$	0.11 ±0.04

[a] γ transitions of the sideband shown in Fig. 2.

In addition, the single-particle alignment plot shows that the aligned angular momentum $i_{\text{s.p.}}$ for the negative-parity band displayed in Fig. 2(b) increases with increasing rotational energy and attains a maximum value at $\hbar\omega\sim 0.14$ MeV. Beyond this rotational frequency there is a sharp quenching of angular momentum alignment. This quenching of $i_{\text{s.p.}}(\omega)$ was interpreted by Nazarewicz [6] to be a manifestation of octupole interaction between the $\Delta j=\Delta l=3$ orbitals. In the ^{153}Eu nucleus the interaction between $d_{5/2}$ and $h_{11/2}$ leads to sharing of the angular momenta between the high-j negative-parity intruder orbital and low-j normal-parity orbitals resulting in a decrease in alignment. At $\hbar\omega=0.26$ MeV, the quenching is maximum. The increase of $i_{\text{s.p.}}(\omega)$ is consistent with the sharp change of $\mathcal{J}^{(2)}$ values [Fig. 2(a)] at frequency above $\hbar\omega\sim 0.30$ MeV.

B. Electric dipole moment

The striking characteristic of the decay of the excited states of the ^{153}Eu nucleus is that $E1$ transitions compete with $E2$ until the high-spin states. Enhancement in low-energy $E1$ transitions could be understood to be due to nucleon polarization inside the nucleus if it attains a reflection asymmetric shape [7]. The $B(E1)/B(E2)$ values derived from the present experiment (given in Table II) indicate that there is an enhancement of these values in the high-spin region particularly at $I>(21/2)\hbar$. This is displayed in Fig. 3(a). At low spin the results agree fairly well with the previously reported values [2]. The intrinsic dipole moment

TABLE III. Experimental $B(E1)/B(E2)$ ratios and dipole moments deduced for high-spin states.

E_γ (keV)	I_i	I_f	$I_\gamma(E1)/I_\gamma(E2)$	$B(E1)/B(E2)$ (10^{-6} fm^{-2})	D_0 e fm
271.9	$29/2^-$	$27/2^+$	0.06 ± 0.02	0.12 ± 0.03	0.128 ± 0.068
565.6		$25/2^-$			
271.7	$23/2^+$	$21/2^-$	0.22 ± 0.04	0.20 ± 0.04	0.160 ± 0.068
473.2		$19/2^+$			
293.2	$27/2^+$	$25/2^-$	0.41 ± 0.12	0.49 ± 0.14	0.264 ± 0.139
530.9		$23/2^+$			
429.3	$29/2^+$	$27/2^-$	0.46 ± 0.03	0.22 ± 0.01	0.172 ± 0.043
556.9		$25/2^+$			

D_0 hence has been calculated for spins $I>(21/2^{\pm})\hbar$ using the particle-rotor-model formulation [5]. The value of Q_0 (=6.75 eb) has been obtained from $Q_{\text{expt}}=2.412\,eb$ [8]. In Table III, D_0 values thus estimated from $B(E1)/B(E2)$ ratios for $I>(21/2)\hbar$ are given. The average dipole moment obtained in the present work is $\langle D_0\rangle=0.181\pm0.007\,e$ fm.

The intrinsic dipole moment D_0 can be expressed as a sum of D_0^{LD} and D_0^{shell}, where D_0^{LD} is obtained from Strutinsky's liquid drop model for a deformed nucleus and D_0^{shell} is due to the quantal shell effects. The D_0^{shell} value for ^{153}Eu has been taken from the interpolated values of D_0^{shell} of ^{152}Sm and ^{154}Gd [9]. Taking $\beta_2=0.2$ and $\beta_4=0.04$ from Ref. [10] and $C_1=0.000\,69$ fm from Ref. [7], the β_3 parameter in the expression of D_0^{LD} [5] has been found to be approximately 0.03. But if the shell effect is assumed to be very small so that D_0^{shell} could be neglected, the β_3 deformation would then be 0.11 from $\langle D_0\rangle_{\text{expt}}$. Depending on the magnitude of shell effect, β_3 lies in the range $0.03\leqslant\beta_3\leqslant0.11$. This is consistent with the large β_3 ($=0.11$) values reported for ^{152}Sm [9,11].

C. Magnetic-dipole moment

In the case of a reflection asymmetric nucleus, the opposite-parity bands originate from the same intrinsic state of mixed parity and thus the magnetic moments should be same for both bands. In order to determine the magnetic moments, the branching ratio of the $E2$ transition, a $\Delta I=2$ crossover transition from a level to that of the $M1$, a $\Delta I=1$ transition, has been derived for each band, which provides the value of the $(g_K-g_R)/Q_0$ parameter, where g_K and g_R are the orbital and rotational g factors and Q_0 is the intrinsic quadrupole moment. The values obtained are plotted in Fig. 3(b). It is to be noted that the values for positive- and negative-parity bands differ in the low-spin region. This is in agreement with the previously reported values [2]. This implies that at low excitation the bands are built on different intrinsic configurations, probably originating from $d_{5/2}$ (for positive parity) and $h_{11/2}$ (for negative parity) orbitals. However, in the high-spin region the $(g_K-g_R)/Q_0$ values for both the bands overlap fairly well within error bars, thus indicating a possible mixing between the two configurations. Taking the average of the $(g_K-g_R)/Q_0$ parameters over the full range of values and $g_R\sim Z/A$ and $Q_0=6.75\,eb$, the moments for the $5/2^{\pm}$ bands have been estimated. The moment for the ground-state positive-parity band with spin $5/2^+$ is found to be $1.71\pm0.12\,\mu_N$ and is in good agreement with the directly measured value $1.533\mu_N$ [12], whereas that for the negative-parity band with spin $5/2^-$ is $2.035\pm0.128\,\mu_N$ which is somewhat lower than the previously reported values $2.24\mu_N$ [2] and $3.22\mu_N$ [12]. In the present work, the moments of both the bands are rather close to each other.

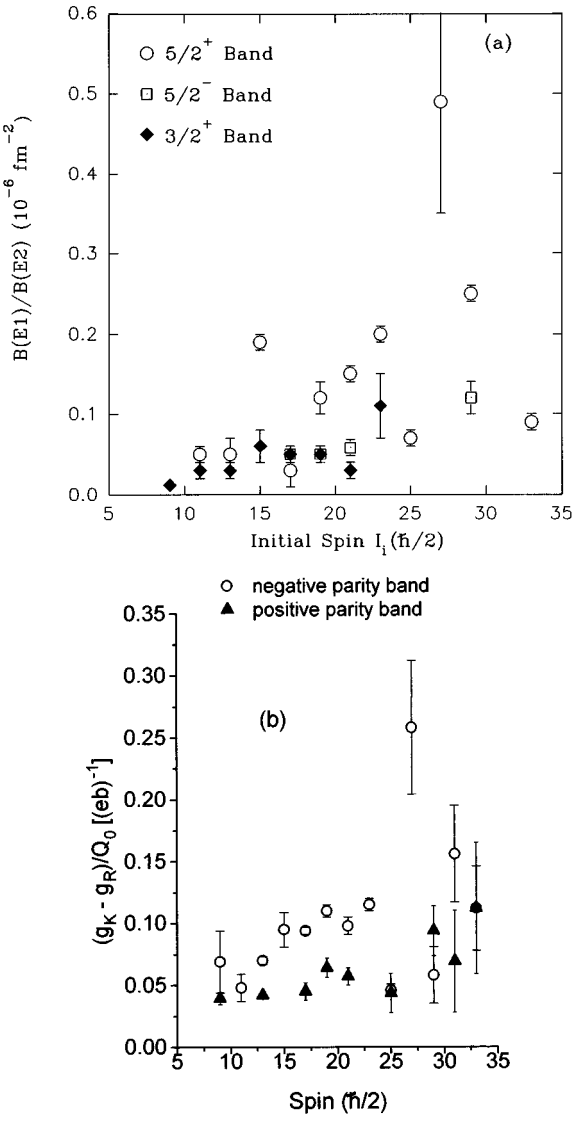

FIG. 3. (a) The $B(E1)/B(E2)$ values shown with spins of the levels. (b) Plots of $(g_K-g_R)/Q_0$ with increasing spin for positive- and negative-parity bands.

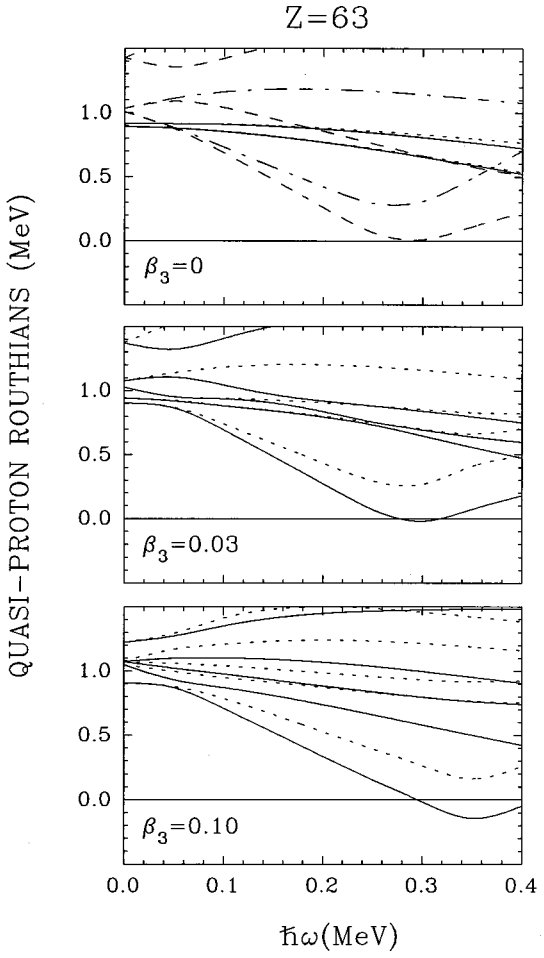

FIG. 4. Routhians for quasiprotons calculated for $Z=63$ for $\beta_3=0.0$, 0.03, and 0.1. The quadrupole and hexadecapole deformations $\beta_2=0.2$ and $\beta_4=0.04$ have been taken from Ref. [10]. The pairing energy gap has been kept constant at $\Delta_p=0.9$ MeV, corresponding to 80% of the odd-even mass difference. Solid lines represent states with simplex $s=+i$, while short-dashed lines $s=-i$. The dash-dotted and long-dashed lines in the $\beta_3=0$ diagram represent states with $\pi=-1$, $\alpha=+i$ and $\pi=-1$, $\alpha=-i$, respectively as defined in Ref. [21].

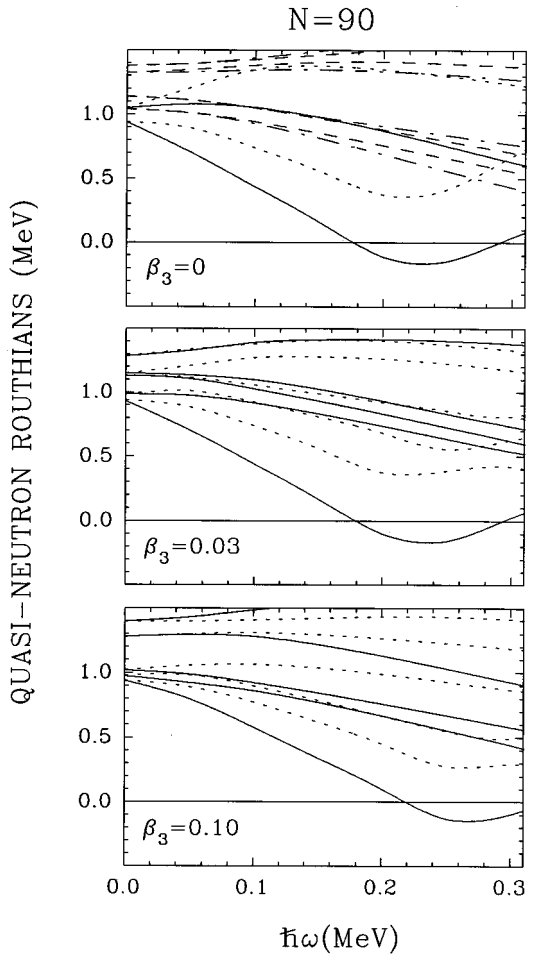

FIG. 5. Similar to Fig. 4, but for neutrons with $N=90$ and $\Delta_n=0.95$.

IV. DISCUSSION

In order to investigate the single-particle structure of ^{153}Eu, a deformed Woods-Saxon calculation with universal parametrization [13] has been performed for the even-even ^{152}Sm core. The calculation with deformation parameters $\beta_2=0.2$ and $\beta_4=0.04$ taken from Ref. [10] shows that the orbitals $\Omega=5/2^{\pm}$ differing by $\Delta l=3$ come close in energy near the proton Fermi surface (the energy difference between these two orbitals is 148 keV). Therefore, there is a probability to have octupole correlated states as the yrast configuration for ^{153}Eu arising from the mixing of $\Omega=5/2$ orbitals of $\pi d_{5/2}$ and $\pi h_{11/2}$ through the Y_{30} term of the nuclear Hamiltonian.

The cranked shell model (CSM) calculations have been carried out with the above-mentioned deformed potential in order to understand the observed high-spin behavior of ^{153}Eu. Figure 4(a) and 5(a) display the quasiparticle Routhians for $Z=63$ and $N=90$, respectively, for $\beta_3=0.0$. The pairing energy gap has been chosen to be 80% of the odd-even mass difference. It should be mentioned here that in the present case of $Z=63$, proton AB crossing is blocked in band 2 due to the presence of the odd proton in the $h_{11/2}$ orbital. For the neutron, the AB crossing occurs at $\hbar\omega_c=0.22$ MeV [shown in Fig. 5(a)], but the observed band crossing is obtained at $\hbar\omega_c\sim0.30$ MeV, which is substantially delayed compared to the theoretical prediction. This high-spin feature has been investigated by performing a representative CSM calculation with fixed β_3 values. The inclusion of the octupole term has been supported by several experimental results, viz., the quenching of single-particle aligned angular momenta with increasing spin, the increase of $B(E1)/B(E2)$ ratios with spin, and the same order of magnitude of $(g_K-g_R)/Q_0$ values at high spin. All these observations seem to indicate that there might be a change of shape from reflection symmetric to reflection asymmetric with the increasing spin. Similar features have been observed in several nuclei in the ''Sm region,'' for example, ^{144}Ce [14], ^{146}Ce [15], ^{146}Nd [16], ^{148}Nd [16,17], ^{148}Sm [18,19], and ^{150}Sm [20] above spin $I=8\hbar$. Therefore, the CSM calculations have been performed at $\beta_3=0.03$ and 0.1. The pairing gaps $\Delta_p=0.9$ MeV and $\Delta_n=0.95$ MeV have been kept constant while β_3 is varied and the diagrams are shown in Figs. 4(b) and 4(c) and Figs. 5(b) and 5(c) for protons and neutrons, respectively. It is found that crossing frequency shifts towards the higher rotational frequency with the increase in β_3 values. The same phenomenon has been found

in ^{224}Th by Nazarewicz and Olanders [21]. The interpretation of this feature could be as follows: As the octupole interaction becomes stronger with increasing β_3, a larger mixing of $\nu f_{7/2}$ with $\nu i_{13/2}$ orbitals delays the crossing frequency due to the increased involvement of the low-j orbitals. Thus the assumption of reflection asymmetric shape for ^{153}Eu at high spin seems to give better agreement between the theoretical calculation and observed crossing frequencies.

The positive-parity sideband (band 3) shows a good rotor behavior and does not undergo any signature splitting. In this band, the proton occupies the $d_{5/2}$ orbital and thus the proton AB crossing is not blocked. It is interesting to note that the calculated proton AB crossing at $\hbar\omega_c = 0.28$ MeV for $\beta_3 = 0$ [Fig. 4(a)] agrees quite well with the observed band crossing in band 3 [Fig. 2(a)]. However, the calculation at $\beta_3 = 0$ predicts the neutron alignment at a considerably lower frequency, i.e., at $\hbar\omega = 0.22$ MeV. It is therefore expected that the first band crossing in the sideband should be due to neutron alignment, which would imply that in the sideband also neutron alignment is delayed. This observation could be interpreted in terms of octupole correlation as in the case of bands 1 and 2. The calculation also shows that with $\beta_3 \neq 0$ the proton AB crossing is further delayed [Figs. 4(b) and 4(c)] and thus will not be observed around $\hbar\omega = 0.28$ MeV. It may be mentioned here that the microscopic calculation of Nosek *et al.* [1] has also predicted parity doublet bands built on $3/2^+$ and $3/2^-$ proton orbitals of ^{153}Eu, where the $3/2^-$ band head lies 530 keV above that of $3/2^+$, while the $5/2^+$ and $5/2^-$ band heads are separated by 90 keV. This may be the reason why the band 1 originating from the mixing of the $5/2^+$ and $5/2^-$ orbitals shows signature splitting and band 3 does not.

V. CONCLUSION

In this work the positive- and negative-parity bands (bands 1 and 2, respectively) of the ^{153}Eu nucleus have been extended to $39/2^+$ and $43/2^-$ spins and are found to be linked by fast $E1$ transitions. The large $B(E1)/B(E2)$ ratios in the high-spin region indicate a finite-β_3 deformation when β_2 and β_4 values are assumed from the systematics of this mass region. In addition, the quenching of angular momentum alignment and the same values of magnetic moment parameters support this result. A representative CSM calculation with finite β_3 gives better agreement with the experimentally observed delayed crossing frequency in bands 1 and 2. The neutron alignment in the positive-parity sideband (band 3) is also delayed, indicating a possible octupole deformation in band 3. However, there is a need to carry out a dynamical calculation in order to investigate the rotational behavior of ^{153}Eu with increasing spin.

ACKNOWLEDGMENTS

We express our deep gratitude to Professor P. N. Mukherjee for stimulating discussions during the course of work. We wish to thank Professor G. K. Mehta and Dr. S. K. Dutta for providing the accelerator and other necessary facilities.

[1] D. Nosek, R. K. Sheline, P. C. Sood, and J. Vasil, Z. Phys. A **344**, 277 (1993).
[2] C. J. Pearson, W. R. Phillips, J. L. Durell, B. J. Varley, W. J. Vermeer, W. Urban, and M. K. Khan, Phys. Rev. C **49**, R1239 (1994).
[3] J. M. Chatterjee, Somapriya Basu, R. K. Chattopadhyay, K. Kar, D. Banik, R. P. Sharma, and S. K. Pardhasaradhi, Z. Phys. A **344**, 149 (1992).
[4] S. S. Ghugre, S. B. Patel, M. Gupta, R. K. Bhowmik, and J. A. Sheikh, Phys. Rev. C **47**, 87 (1993).
[5] M. Dahlinger, E. Kankeleit, D. Habs, D. Schwalm, B. Schwartz, R. S. Simon, J. D. Burrows, and P. A. Butler, Nucl. Phys. **A484**, 337 (1988).
[6] W. Nazarewicz, in *Nuclear Structure*, Niels Bohr Centennial Conferences 1985, edited by R. Broglia, G. Hagemann, and B. Herskind (North-Holland, Amsterdam, 1985), p. 263.
[7] G. A. Leander, W. Nazarewicz, G. F. Bertsch, and J. Dudek, Nucl. Phys. **A453**, 58 (1986).
[8] Y. Tanaka, R. M. Steffen, E. B. Shera, W. Reuter, M. V. Hoehn, and J. D. Zumbro, Phys. Rev. Lett. **51**, 1633 (1983).
[9] W. Nazarewicz and S. L. Tabor, Phys. Rev. C **45**, 2226 (1992).
[10] R. Bengtsson, S. Frauendorf, and F. R. May, At. Data Nucl. Data Tables **35**, 15 (1986).
[11] H. Soloviov, *Theory of Complex Nuclei* (Nauka, Moscow, 1971); *Structure of Doubly Even Deformed Nuclei* (Nauka, Moscow, 1974).
[12] M. A. Lee, Nucl. Data Sheets **60**, 419 (1990).
[13] S. Cwiok, J. Dudek, W. Nazarewicz, J. Skalski, and T. Werner, Comput. Phys. Commun. **49**, 379 (1987).
[14] A. S. Mowbray, J. B. Fitzgerald, J. L. Durell, M. A. C. Hotchkis, W. R. Phillips, and B. J. Varley, Daresbury Laboratory Annual Report No. 1988-89, pp. 22 and 23 (unpublished).
[15] W. R. Phillips, R. V. F. Janssens, I. Ahmad, H. Emling, R. Holtzmann, T. L. Khoo, and M. W. Drigert, Phys. Lett. B **212**, 402 (1988).
[16] W. Urban, R. M. Lieder, W. Gast, G. Hebbinghaus, A. Krämer-Flecken, T. Morek, T. Rzaca-Urban, W. Nazarewicz, and S. L. Tabor, Phys. Lett. B **200**, 424 (1988).
[17] R. Ibbotson, B. Kotlinski, D. Cline, K. G. Helmer, A. E. Kavka, A. Renalds, E. G. Vogt, P. A. Butler, C. A. White, R. Wordsworth, and D. L. Watson, Nucl. Phys. **A530**, 199 (1991).
[18] E. Hammaren, E. Liukkonnen, M. Piiparinen, J. Kownacki, Z. Sujkowski, Th. Lindblad, and H. Ryde, Nucl. Phys. **A321**, 71 (1979).
[19] W. Urban, R. M. Lieder, J. C. Bacelar, P. P. Singh, D. Alber, D. Balabanski, W. Gast, H. Grawe, G. Hebbinghaus, J. R. Jongman, T. Morek, R. F. Noorman, T. Rzaca-Urban, H. Schnare, M. Thoms, O. Zell, and W. Nazarewicz, Phys. Lett. B **258**, 293 (1991).
[20] W. Urban, R. M. Lieder, W. Gast, G. Hebbinghaus, A. Krämer-Flecken, K. P. Blume, and H. Hübel, Phys. Lett. B **185**, 331 (1987).
[21] W. Nazarewicz and P. Olanders, Nucl. Phys. **A441**, 420 (1985).